ZIBELINE INTERNATIONAL™ PUBLISHING

ISSN: 2773-6202 (Online)
CODEN: JTIOCC

Journal of Technology & Innovation (JTIN)

DOI: http://doi.org/10.26480/jtin.02.2023.47.53

REVIEW ARTICLE

RESEARCH ON NUMERICAL SIMULATION OF PCCI ENGINE: A REVIEW

Pham Minh Tuan[a], Cao Dao Nam[b,*]

[a]School of Mechanical Engineering, Hanoi University of Science and Technology, Hanoi, Vietnam.
[b]Institute of Mechanical Engineering, Ho Chi Minh City University of Transport, Ho Chi Minh City, Vietnam.
[*]Corresponding Author Email: nam.cao@ut.edu.vn

ARTICLE DETAILS

Article History:

Received 12 December 2022
Revised 20 April 2023
Accepted 01 May 2023
Available online 17 May 2023

ABSTRACT

The global environment is being affected by the use of fossil fuels to provide energy for internal combustion engines (ICE) due to a large amount of CO_2 emission. Specific toxic substances are NOx, and CO, soot, particulate matter that exists in the environment at high densities while having a global impact. The automotive industry of countries worldwide is constantly changing and evolving to discover new solutions that reduce fuel use while developing cleaner and more advanced combustion methods, which as a low-temperature combustion engine (LTC). This study uses computational fluid dynamics (CFD) to understand partial pre-mixed compression combustion (PPCI), with HCCI and RCCI being advanced low-temperature combustion concepts. Lowering the average combustion temperature is an advantage of PCCI; it optimizes CO and NOx emission rates while maintaining high thermal efficiency. Investigate the intake pattern, including flame length, mixing pulse, and intake air volume, to determine the importance of that factor for oxidation using the LES. Studies have been performed using RANS and LES models to stimulate mixing and combustion.

KEYWORDS

PPCI, LTC, CFD, ICE

1. INTRODUCTION

When it comes to conventional diesel combustion (CDC), the fuel injection process is delayed; it continues in the combustion process (incomplete combustion). Resulting in a large amount of these emissions and the need for a post-treatment system (Zehni et al., 2020; Soloiu et al., 2015). The combustion temperature must be reduced to avoid the generation of soot and NOx (Nibin et al., 2021). The usual method to reduce the combustion temperature is to use an exhaust gas recirculation (EGR) system (Park et al., 2015; Pandey et al., 2018; Bhurat et al., 2021). In addition, the other method is more difficult to increase the early injection angle to give more pre-mix time to help the fuel and air achieve a better mixing composition. Therefore, the combustion temperature is lower. Besides, hydrocarbon gas (UHC) and CO are not completely burned when the combustion temperature is reduced, which can affect the combustion efficiency. In SCCI mode, to overcome the HCCI mode's restriction, deliberate thermal or fuel stratification is used. It's not complicated for direct fuel injection to stratify fuel in the combustion chamber, and all of the technologies required to do so are currently available (Wang et al., 2019; Yoon et al., 2018). This combustion mode is frequently known as partial pre-compression combustion (PPCI) or sometimes shortened as partial pre-mix combustion (PPC), which uses direct fuel injection to regulate the fuel injection timing mixing time (Bhave et al., 2020; D'Ambrosio et al., 2016). PPCI is an intermediate process that combines conventional diesel combustion with the HCCI combustion mode (Zheng et al., 2019). Previously, research on PPCI engines focused on investigating the engine parameter, which controls the mixture composition and exhaust output. Combustion stability and engine load range must be considered as the combustion rate increases. CFD simulation to analyze mixtures, mixture combustion temperature, and flame-wall interactions to improve the efficiency of PPCI engines (An et al., 2017; Fukushima et al., 2015). All three basic combustion modes can coexist in PPC engines: ignition forward spread, premixed flame, and unmixed flame. Given the difficulties in implementing combustion methods from a numerical aspect, it is crucial and pivotal to assess which combustion regimen is being implemented. This work shows the difference between combustion with pre-mixing and combustion without pre-mixing (Mei et al., 2017). It was known to be more difficult and often required detailed numerical simulation (DNS) when studying the difference between pre-mixing and without pre-mixing. According to Musculus et al., most of mixture was ignited in the mixed combustion mode before the PPCI injection time is increased. Figure 1 illustrates a model of PPCI combustion and CDC self-ignition (Musculus et al., 2013).

The injection's position and time are the most important factors in forming the premix. Due to the non-volatility of diesel, direct fuel injection is more commonly employed to ignite the premix (Natarajan et al., 2017). In PPCI mode, two alternative direct injection methods are used for the injection time of conventional diesel engines: early direct injection and delayed direct injection. Fuel is delivered directly into the cylinder during the compression stroke in early direct injection (Eguz et al., 2014), allowing adequate fuel and air to mix before the top dead center. The common combustion process with early direct fuel injection is premix and compression combustion (PCCI).

2. WAVE PRE-COMBUSTION, PRE-MIXED FLAME, UNMIXED FLAME

Diesel PPCI has drastically different combustion and exothermic characteristics than conventional diffusion-controlled combustion engines. Due to high dilution and premixing as well as relative cooling of the combustion gas in the cylinder (due to EGR), the initial ignition reactions in LTC mode are slower than conventional diesel combustion (Pandey et al., 2021; Zehni et al., 2017). Partial pre-combustion is a combination of pre-mixed and unmixed pre-combustion. Premix combustion occurs when fuel and air coexist before starting combustion in a completely homogeneous zone or a stratified zone consisting of dilute fuel-air mixtures or bold fuel-air mixtures. When fuel and air mix during

Quick Response Code	Access this article online	
	Website: www.jtin.com.my	DOI: 10.26480/jtin.02.2023.47.53

Cite The Article: Pham Minh Tuan, Cao Dao Nam (2023). Research on Numerical Simulation of Pcci Engine: A Review. *Journal of Technology & Innovation, 3(2): 47-53.*

combustion, it is pre-mixed combustion, which means that fuel and air are directed separately into the combustion chamber. Therefore, PPCI is also used regardless of stratification conditions, whether the combustion mode is pre-mixed or not pre-mixed (Bilger et al., 2005). In general, to improve the PPCI engine's model, we have to compare two different premix combustion methods, namely combustion front spread and premixed flame front spread. The propagating transition is a chain of separate self-ignition points regardless of the mass of the mixture and the mixture's temperature when it enters the combustion chamber. However, the combustion reaction rate depends on the ignition delay time τ_{ig} which is varied by thermodynamic states, including three main factors: temperature, pressure, equivalence ratio (Fuyuto et al., 2014).

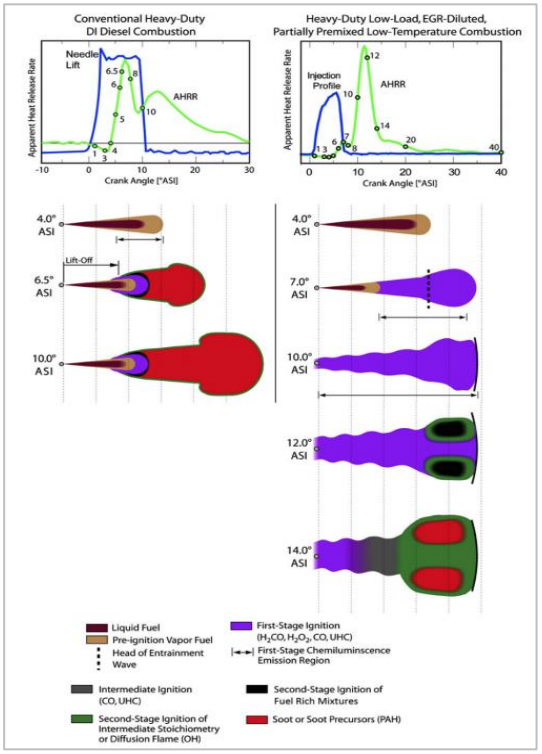

Figure 1: Phenomenal model of PPCI combustion and CDC self-ignition (Singh et al., 2017)

$$\tau_{ig} = f(T, P, \phi) \quad (1)$$

In pre-combustion mode, the flame mixes first if additional heat and mass transfer are required, in the form of diffusion, into the combustion chamber to continue the combustion. The spread of the premixed flame is greatly influenced by the perturbation structure depicted in the famous Borghi diagram (Bhagatwala et al., 2015). The turbulence acts indirectly when propagating the combustion. The disturbance governs the mixing and hence the local and proportional temperature distribution equivalent before combustion. When combustion occurs, the integrated chaos scale is slower than the chemical scale. Studies that provide for PPCI-related conditions have been carried out within the framework of DNS, showing that premixed flame can occur simultaneously but that the combustion mode is likely to be the dominant combustion mode (Zhang et al., 2015; Singh et al., 2018).

There are two diesel LTC options, called RCCI and PCCI. In RCCI combustion, a slow-reactive fuel (such as gasoline) is pre-mixed, and fuel with high reactivity (such as diesel) is injected directly to create a split reaction in the cylinder. Partial combustion of the diesel premix is known as PCCI. Three types of PCCI alternatives use gasoline: (i) partial fuel stratification (PFS), (ii) medium fuel stratification (MFS), and (iii) high fuel stratification (HFS). Figure 2 shows the temperature of fuel stratification in the combustion chamber. In the PFS embodiment, either the injector or direct fuel injection is used to prepare a uniform intake very early, and stratification is generated by directly injecting a small volume of fuel afterward (Beatrice et al., 2009). The stratification is made so that spontaneous combustion occurs continuously while keeping the NOx and soot emissions super low (Zhang et al., 2015). In **Figure 2**, The PPCI combustion method is an intermediate method of HCCI and CDC. In different injection methods, the degree of fuel stratification will not be the same; this also has a different effect on the total heat from pre-mixed and non-premixed combustion. The different degrees of stratification and the amount of bold fuel mixture will increase the importance of the combustion method. The fuel stratification is determined by calculating the local equivalent proportional distribution defined by Equation (2) (Zhang et al., 2017; Rohani et al., 2016):

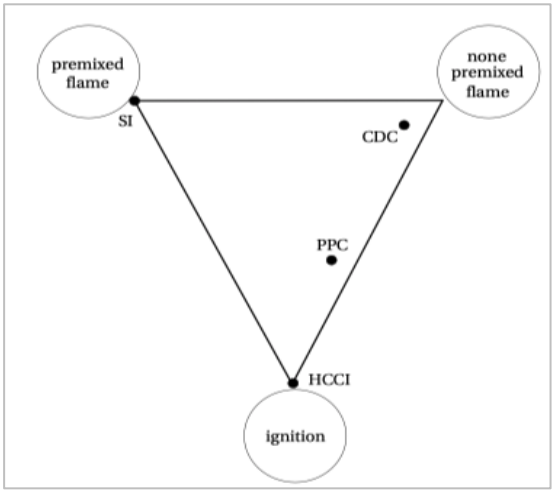

Figure 2: The basic combustion methods are divided into three directions. The engine concept is determined based on the influence of each burning mode on the total heat output (Elzahaby et al., 2018)

$$\phi = \left(\frac{m_f}{m_a}\right) / \left(\frac{m_f}{m_a}\right) \quad (2)$$

With components: m_f being the regional mass of the fuel; m_a being the regional mass of the air, and s representing the stratified measurement. The value > 1 corresponds to the condition of rich fuel, the value < 1 corresponds to the condition of low fuel, and the value = 1 corresponds to the ideal condition. It can be seen in **Figure 3** that the structure of ϕ in the PPC concept is much broader than that of the HCCI engine concept (Soloju et al., 2018).

NOx-soot formation and the oxidation of carbon black depend on combustion temperature and local equivalent ratio in the cylinder. The fuel determines the size and shape of the soot-forming area in the ϕ -T map.

3. The Turbulence of The Flow

Laminar flow is complex with no mixing of liquid particles and without velocity and pressure pulses. With the laminar motion of the liquid in a straight tube of constant cross-section, all lines are directed parallel to the axis of the tube, with no horizontal displacement of the fluid (Schmitt, 2007). However, laminar motion cannot be considered non-moving, for although there is no visible vortex in it, simultaneously with the translational motion, there is an ordered rotation of the individual fluid particles around their instantaneous centers with some angular velocity (Elkelawy et al., 2021). Turbulent flow is characterized by vigorous fluid mixing and pulses of velocity and pressure. Transverse displacement and rotation of individual liquid volumes occur in turbulent flow, along with the primary longitudinal displacement of the liquid (Liang et al., 2021; Salahi et al., 2019). Cyclones are distinguished by scales showing different shapes and changes over eddy currents. The integral scale is the scale with the highest energy content the characteristics of length l_o, velocity u_p, and time τ_o. The Reynolds number over time is (Sone et al., 2003; Parks et al., 2010):

$$Re_0 = \frac{u_0 l_0}{\nu}, \tau_0 = \frac{l_0}{u_0} \quad (3)$$

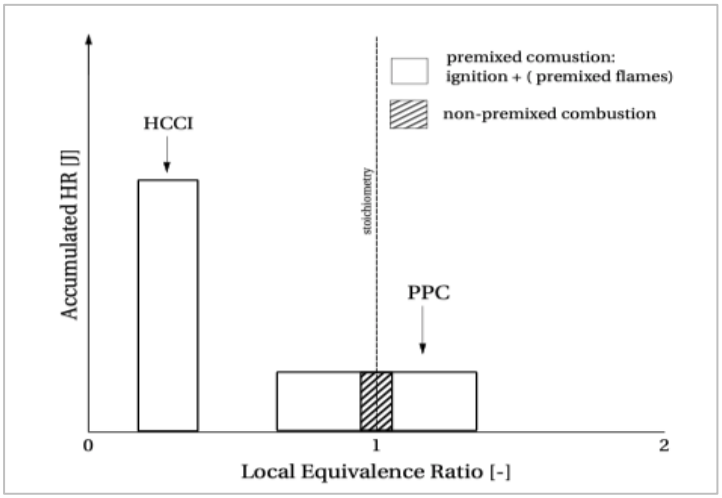

Figure 3: Proposed conceptual model of the distribution of heat released in the combustion cycle depending on the equivalent ratio and combustion model (Lundgren, 2017).

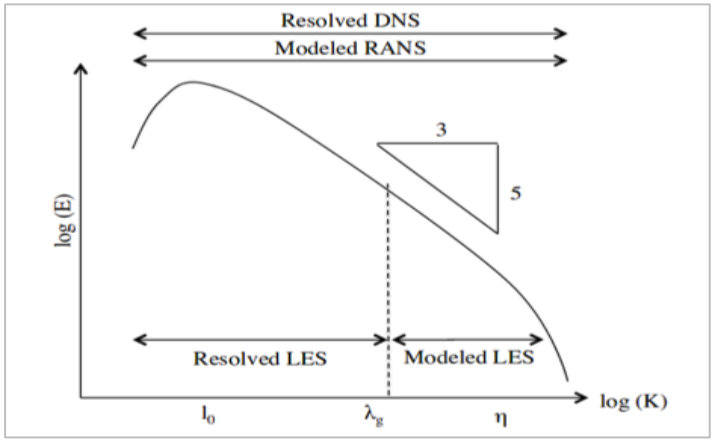

Figure 4: The modeled diagram of the noise kinetic energy for the RANS, LES, and DNS models (Sabelnikoy et al., 2013).

With components: ν is the kinematic viscosity. The smallest chaos scale is the Kolomogrov scale, which defines eddy currents with the least amount of energy at the location where chaotic kinetic energy is dissipated as heat. The Kolomogrov scale of flame length, flame velocity, and flame time is defined by the formula (4) (Hoang et al., 2022; Chomiak et al., 1996; D'Ambrosio et al., 2015):

$$l_\eta = \left(\frac{\nu^3}{\varepsilon}\right)^{1/4}, u_\eta = (\nu\varepsilon)^{1/4}, \tau_\eta = \left(\frac{\nu}{\varepsilon}\right)^{(1/2)} \quad (4)$$

With components: ε is the dispersion of chaotic kinetic energy. The energy scale principle proposed by LF Richardson specifies the decomposition of large vortices with the highest energy levels into the smallest energy levels by reducing their energy until reaching the dispersed molecule and finally converted into heat. RANS and LES are two models used to model the perturbation scales. The energy flow associated with RANS and LES models is depicted in **Figure 4** (Zhang et al., 2014).

4. U-Rans Formula

According to formula (5), a stream quantity ϕ can be divided into two parts in the U-RANS model: meantime $\bar{\phi}$ and oscillation ϕ'' (Lo¨ rstad et al., 2010; Jia et al., 2013):

$$:\phi = \bar{\phi} + \phi'' \quad (5)$$

Since the reaction density varies, Favre's formula is used:

$$\tilde{\phi} = \frac{\overline{\rho\phi}}{\bar{\rho}} \quad (6)$$

The average time of the U-RANS equations assuming Le = 1 is:

$$\frac{\partial \bar{\rho}}{\partial t} + \frac{\partial \bar{\rho}\tilde{u}_j}{\partial x_j} = \bar{S}_\rho \quad (7)$$

$$\frac{\partial \bar{\rho}\tilde{u}_i}{\partial t} + \frac{\partial \bar{\rho}\tilde{u}_i\tilde{u}_j}{\partial x_j} = -\frac{\partial \bar{p}}{\partial x_j} + \frac{\partial \bar{\tau}_{ij}}{\partial x_j} - \frac{\partial \bar{\rho}\widetilde{u_i''u_j''}}{\partial x_j} + \bar{S}_{u_i} \quad (8)$$

$$\frac{\partial \bar{\rho}\tilde{h}}{\partial t} + \frac{\partial \bar{\rho}\tilde{u}_j\tilde{h}}{\partial x_j} = -\frac{\partial \bar{p}}{\partial t} + \frac{\partial}{\partial x_j}\left(\bar{\rho}\tilde{\alpha}\frac{\partial \tilde{h}}{\partial x_j}\right) - \frac{\partial \bar{\rho}\widetilde{h''u_j''}}{\partial x_j} + \bar{S}_h \quad (9)$$

$$\frac{\partial \bar{\rho}\tilde{Y}_k}{\partial t} + \frac{\partial \bar{\rho}\tilde{u}_j\tilde{Y}_k}{\partial x_j} = \frac{\partial}{\partial x_j}\left(\bar{\rho}\tilde{D}\frac{\partial \tilde{Y}_k}{\partial x_j}\right) - \frac{\partial \bar{\rho}\widetilde{Y_k''u_j''}}{\partial x_j} + \bar{\rho}\tilde{\omega}_k + \bar{S}_{Y_k} \quad (10)$$

According to the Boussinesq conjecture, Reynolds' tensile stress can be written as (Srihari et al., 2017):

$$-\bar{\rho}\widetilde{u_i''u_j''} = \mu_t\left(\frac{\partial \tilde{u}_i}{\partial x_j} + \frac{\partial \tilde{u}_j}{\partial x_i} - \frac{2}{3}\frac{\partial \tilde{u}_k}{\partial x_k}\delta_{ij}\right) - \frac{2}{3}\bar{\rho}k\delta_{ij} \quad (11)$$

The k - ε model is a perturbation model, which is used to calculate the perturbation viscosity μ t is defined as (Murata et al., 2009):

$$\mu_t = \bar{\rho}C_\mu\frac{k^2}{\varepsilon} \quad (12)$$

With components: k is the perturbation kinetic energy; ε is the dispersion rate; C μ constant model. Their perturbation to the mass of the mixture and the temperature of the mixture are modeled with the uprise diffusion method as follows (Singh et al., 2020):

$$-\bar{\rho}\widetilde{Y_k''u_j''} = \frac{\nu^{sgs}}{Sc^{sgs}}\frac{\partial \tilde{Y}_k}{\partial x_j} \quad (13)$$

$$-\bar{\rho}\widetilde{h''u_j''} = \frac{\nu^{sgs}}{P_r sgs}\frac{\partial \tilde{h}}{\partial x_i} \quad (14)$$

5. LES FORMULA

G space is used in the LES model to resolve certain perturbation scales. The selected variables can be written as (Maghbouli et al., 2015; Jia et al., 2011):

$$\bar{\phi}(x,t) = \int G(r,x)\phi(x-r,t)dr \quad (15)$$

The selection function G must match the basic condition ∫G(r, x) dr = 1. The Favre formula is used as

$$\tilde{\phi} = \frac{\overline{\rho\phi}}{\bar{\rho}} \quad (16)$$

In the LES model, the variable ϕ is resolved by $\tilde{\phi}$ and the variable ϕ'' is unresolved (sub-grid). The tuning equations for the reactive multiphase current in the LES framework can be constructed as follows (Jain et al., 2017):

$$\frac{\partial \bar{\rho}}{\partial t} + \frac{\partial \bar{\rho}\tilde{u}_j}{\partial x_j} = \bar{S}_\rho, \quad (17)$$

$$\frac{\partial \bar{\rho}\tilde{u}_i}{\partial t} + \frac{\partial}{\partial x_j}\left[\bar{\rho}\tilde{u}_i\tilde{u}_j - \bar{\tau}_{ij} - \tau_{ij}^{sgs}\right] = \bar{S}_{u_i} \quad (18)$$

$$\frac{\partial \bar{\rho}\tilde{Y}_k}{\partial t} + \frac{\partial \bar{\rho}\tilde{u}_j\tilde{Y}_k}{\partial x_j} - \frac{\partial}{\partial x_j}\left[\bar{\rho}\tilde{D}\frac{\partial \tilde{Y}_k}{\partial x_j} + \Phi_{Y_k}^{sgs}\right] = \bar{S}_{Y_k} + \tilde{\omega}_k \quad (19)$$

$$\frac{\partial \bar{\rho}\tilde{h}}{\partial t} + \frac{\partial \bar{\rho}\tilde{u}_j\tilde{h}}{\partial x_j} - \frac{\partial}{\partial x_j}\left[\bar{\rho}\tilde{\alpha}\frac{\partial \tilde{h}}{\partial x_j} + \Phi_h^{sgs}\right] = \frac{\partial p}{\partial t} + \bar{S}_h \quad (20)$$

With components: $\bar{S}_\rho, \bar{S}_{u_i}, \bar{S}_{Y_k}, \bar{S}_h$ are selected terms such as mass, momentum, types, and enthalpy equations between the gas and liquid phases.

Sub-grid concepts, concept - sgs, continue to require closed modeling. Selected stress tension obtained from resolved tension rate $\bar{S}_{ij}$ and pressure according to the formula (21) (Pei et al., 2015; Splitter et al., 2010):

$$\bar{\tau}_{ij} = -\bar{p}\delta_{ij} + 2\bar{\mu}\left(\tilde{S}_{ij} - \frac{1}{3\tilde{S}_{kk}\delta_{ij}}\right) \quad (21)$$

The sub-grids tensile stress is modeled using a one-equation vortex (Shim et al., 2020).

$$\tau_{ij}^{sgs} = 2\bar{\rho}\nu^{sgs}\left(\tilde{S}_{ij} - 1/3\tilde{S}_{kk}\delta_{ij}\right) - 2/3\bar{\rho}k^{sgs}\delta_{ij} \quad (22)$$

where the sub-grid viscosity is modeled according to (23)

$$\nu^{\text{sgs}} = C_\nu\sqrt{k^{sgs}}\bar{\Delta} \quad (23)$$

Where $\bar{\Delta} = V_{\text{cell}}^{1/3}$.

Unreleased kinetic energy k^{sgs} according to the following transport formula:

$$\frac{\partial \bar{\rho}k^{sgs}}{\partial t} + \frac{\partial \bar{\rho}\tilde{u}_j k^{sgs}}{\partial x_j} = \tau_{ij}^{sgs}\frac{\partial \tilde{u}_i}{\partial x_j} - D^{sgs} + \frac{\partial}{\partial x_j}\left(\bar{\rho}\frac{\nu^{sgs}}{Pr^{sgs}}\frac{\partial k^{sgs}}{\partial x_j}\right) + \dot{W}^s \quad (24)$$

In which W is the term spray disturbance. Modeling the kinetic energy dissipation of the sub-grid:

$$D^{sgs} = C_\epsilon\bar{\rho}k^{sgs3/2}/\bar{\Delta} \quad (25)$$

According to Sone and Menon, the model coefficients Cv and Cϵ are set to 0.05 and 0.3. Components containing sgs are modeled by the uprise diffusion method

$$\Phi_{Y_k}^{sgs} = \bar{\rho}\frac{\nu^{sgs}}{Sc^{sgs}}\frac{\partial \tilde{Y}_k}{\partial x_j} \quad (26)$$

$$\Phi_{h_s}^{sgs} = \bar{\rho}\frac{\nu^{sgs}}{Pr^{sgs}}\frac{\partial \tilde{h}_s}{\partial x_j} \quad (27)$$

The chemical source term $\tilde{\omega}$k for the k-types in this paper is treated by the WSR and PaSR approaches.

6. BURNING PATTERNS

Model the conversion of energy into heat using kinetic-chemical theory. A complete reaction is constructed as follows (Kiplimo et al., 2012):

$$F + Ox \rightarrow Pr \quad (28)$$

According to the Arrhenius formula, the reaction is regulated by the reaction rate k

$$k = AT^b\exp\left(-\frac{E_A}{R_uT}\right) \quad (29)$$

Components: A is the pre-exponential constant; R_u is the spectral gas constant; E_A is the activation energy, and T is the temperature (Kanda et al., 2005).

7. WSR

According to the Arrhenius formula, the chemical term in each type of equation is established in the form of a formula as follows (Norhafana et al., 2018; Torregrosa et al., 2013):

$$\bar{\omega}_F = A\tilde{T}^b\left[\tilde{X}_F\right]^n\left[\tilde{X}_{Ox}\right]^m\exp\left(-\frac{E_A}{R_u\tilde{T}}\right) \quad (30)$$

The above formula, input from the solved part of the steam calculation formula, the no-subgrid burning model is included. This is the approach, the well-stirred reactor (WSR). In addition, in different conditions, PPCI engines use partially stirred reactors (PaSR) (Kokjohn et al., 2010).

8. PASR

Chomiak and Karlsson propose a partially mixed reactor approach to representing the combustion zone in the CFD element. That means there is only a certain amount of mixture inside the reacting element. The reaction proportional to the ratio between the mixing time scale and the chemical mixture τ_c and τ_{mix} is

$$\tilde{\omega}_k(T, Y_k) = \kappa\dot{\omega}_k\left(\tilde{Y}_k, \tilde{T}\right) \quad (31)$$

$$\kappa = \frac{\tau_c}{\tau_c + \tau_{\text{mix}}} \quad (32)$$

$$\tau_{\text{mix}} = C_{\text{mix}}\sqrt{\frac{k}{\epsilon}\left(\frac{\nu}{\epsilon}\right)^{1/2}} \quad (33)$$

Sabelnikov and Fureby, based on the PaSR model, develop different combustion models. The modified PaSR model proposed by Amin et al. in which a transformation function is applied based on the stratification of the mixture to evaluate whether the reaction level is bounded or not (Hanson et al., 2010).

9. METHODOLOGY

This section will introduce the simulation implementation process, such as initial boundary conditions, and mesh construction.

10. GRID TECHNIQUE

For linear static problems, we can usually solve them with global grid conditions and obtain acceptable results in terms of both computation time and accuracy. For dealing with dynamic or nonlinear problems, the solutions to these problems are very sensitive to mesh quality (Mao et al., 2019). With poor-quality meshes, simulations can give inaccurate results. In addition, since dynamic problems and nonlinear problems require a lot of computing resources, poor mesh quality can make the simulation more difficult and result in poor results, with a long computation time. For the nonlinear problem, the simulation time can be improved by improving the mesh quality leading to easy convergence. Conversely, it can be difficult to converge because of unacceptable mesh quality. In the short term, mesh quality is a good or bad problem for the solution and a matter of success or failure. Failure for the problem (accuracy and runtime). What complicates the meshing inside the engine is how different motion mesh techniques are used to reproduce piston movement while also meeting the mesh requirements for fuel injection. One known method is the "addition and subtraction" method established by the Polimi group. This technique involves adding or subtracting a layer of elements based on the selected elements' longitudinal elongation as the piston moves. Then, the CFD elements in the fuel injection zone are not changed, which helps to improve simulation accuracy and stability. The direction of CFD elements relative to the spray angle is also high. In reference, the spray pattern gives higher results if the CFD plots are adjusted for the injection direction (Ibron et al., 2019). The alternative method is uniform or adjusted deformation of elements, i.e. "transform". The limitation of the transform method is the profound requirement of remapping between grid nodes when the CFD cells are heavily distorted, which reduces the accuracy of the simulation. The alternative method, known as sink boundary, uses piston topology to cut Cartesian cells outside the computational area. This technique gained popularity due to its better durability and less expensive to prepare the mesh than the other two methods. Another technique related to motor mesh is the automatic mesh reconstruction (AMR) method) (Parthasarathy et al., 2020). The method shows that the number of elements in the area will be optimally calculated, by reselecting the essential part of the method, depending on specific conditions, for example, temperature uprise or specific reaction level. Therefore, a combined method using uniform transformation of cells with alignment in the direction of spray is optimal.

11. BOUNDARY CONDITIONS

The system of Euler equations together with the continuity equation form a complete system of dynamic equations for the ideal fluid, allowing us to define the field of the hydrodynamic variables to be sought – pressure p, and velocity vector components u, v, w. It is an elliptical system of partial differential equations, and to find a solution, initial and boundary conditions must be given (Van Alstine et al., 2012). Initial conditions – conditions for the pressure and velocity fields at the initial time (t=0). The functions ... have any degree because they satisfy the compatibility condition in each specific problem. Note that initial conditions are only necessary if the flow is non-stationary, but they are not necessary for stationary (stationary) flow. The boundary condition is a condition that must be satisfied for the solution of the problem at each time, and it depends on each specific problem. The engine simulations performed involve the simulation of the "closed cycle", which is the time from closing the inlet valve (IVC) to the opening of the outlet valve (OVO). Therefore, the difficulty is determining the stream conditions created by the inlet valves (IVC). One practice seen in closed-loop simulation is to use the rotation of a rigid body to represent vortex and turbulent motion (Prikhodko et al., 2012). The influence of initial steam conditions on mixing in PCCI engines has been studied by Ibron et al., It has been shown that perturbation caused by injection is much more advantageous than perturbation produced by the flow of the intake valve. But for PPCI engines, this may fail due to uneven mixing, particularly for advanced injection timing. The inlet conditions change such as intake air temperature and air pressure, cylinder wall temperature, mix ingredients (in the case of EGR), and the number of cylinders. On the other hand, it is necessary to define boundary conditions for fuel injection, such as fuel volume, spray speed, spray pressure, and injection start time. **Figure 5** presents the local equivalent scale and temperature fields for SOI -17.5. Although the injection time is quite late, at the beginning of combustion, the mixture composition is in the range of $0.3 < \phi < 0.7$, which means that all mixtures are poor. Therefore, the combustion mode is a pre-mix mode, the same as a PCCI engine. The sprayed fuel acts on the top of the piston to create an upward vortex that pushes the gaseous mixture toward the cylinder cover. The center of fire starts with the thinnest mixtures and spreads along with the richer mixtures.

The feed temperature requested for CA-50 increased to 28°K when the spray time slowed to SOI-3. The result is the equivalent ratio and temperature distribution shown in **Figure 6**. In this situation, the order of combustion is the same as in a regular CDC cycle. Most of the mixture will be mixed before starting to burn due to the miscibility and prolonged burning time caused by the cooling process (Dumitrescu et al., 2012). Furthermore, the partially premixed mixtures had sufficient mixing time to blend better near or below the layering measurement (white line). Therefore, the mixed composition formed in SOI-3 will rapidly increase the pressure rise rate (Ewphun et al., 2020). The injection pressure is less than 800 bar, which is a normal Diesel cycle, and in the case of a high spray pressure of 1600 bar, it is a typical PPCI cycle - partial pre-mixed compression combustion. Due to the higher injection pressure, the injection time is reduced to preserve the injected fuel quantity (Bhiogade et al., 2017).

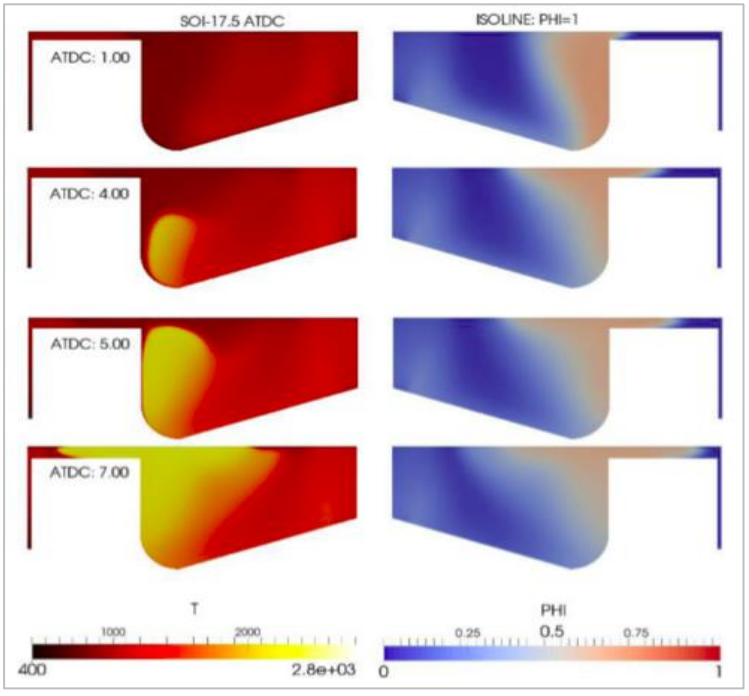

Figure 5: Image of temperature distribution and equivalent scale for the case: SOI -17.5 ATDC, P_{in} = 2.15 bar, T_{in} = 452°K (Karthickeyan et al., 2020)

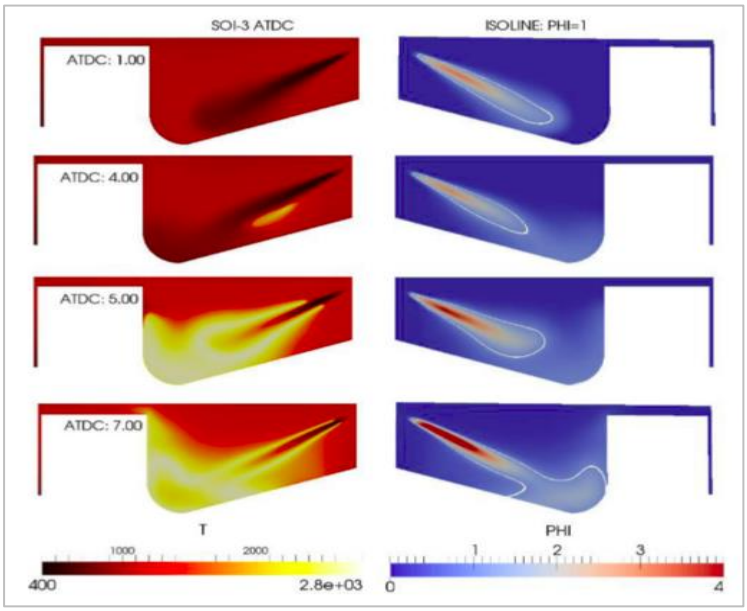

Figure 6: Image of temperature distribution and equivalent scale for the case: SOI -3.0 aDTC, P_{in} = 2.15 bar, T_{in} = 480°K (Singh et al., 2017)

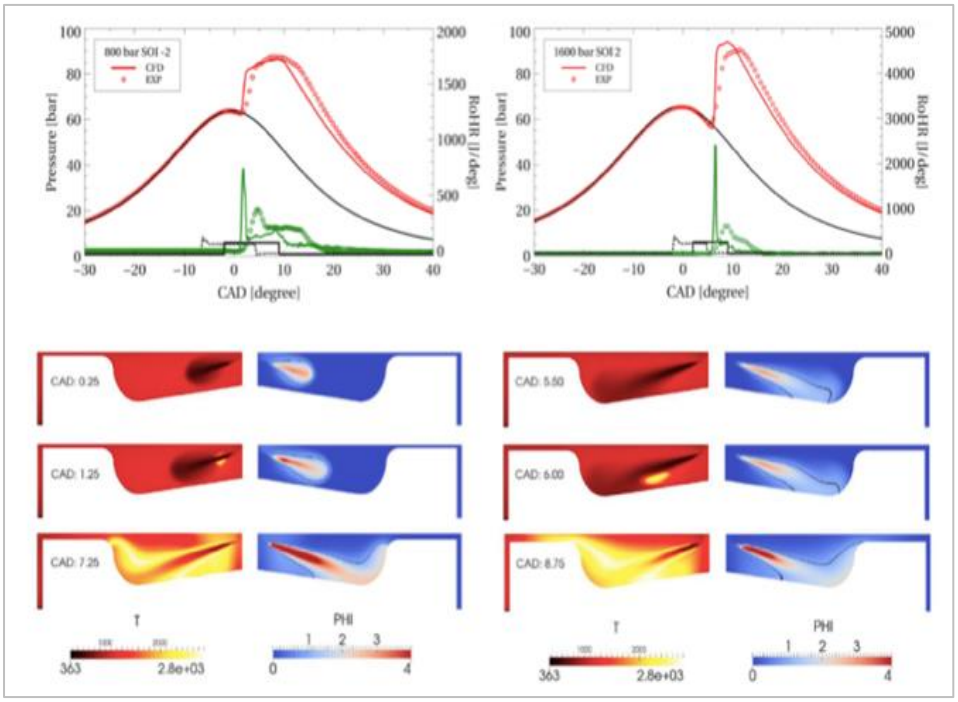

Figure 7: Distribution image Pressure and distribution of fuel and temperature for 800 bar injection case (left) and 1600 bar injection case (right) (Sankaralingam et al., 2018).

Figure 7 shows the pressure and temperature distributions and equivalent ratios for these two cases during combustion. At the start of combustion, it is 1.25 CAD with a pressure of 800 bar and 6 CAD with a pressure of 1600 bar, the injector equilibrium region, is much larger in the case of higher injection pressure. Mixed products containing a large amount of premix at the percentile mixture will lead to rapid burning at high temperatures and thus increase the rate of NOx formation (Satishkumar et al., 2021). The delayed combustion is in the case of high injection pressure. High cetane diesel oil injection will not cause prolonged late fire due to the higher diesel spray pressure.

12. Conclusion

The probable existence of all fundamental combustion modes, such as ignition forward propagation, and pre-mixed and non-premixed propagation, has made the CFD modeling of PPCI engines difficult. We solely discriminate between pre-mix and non-premix combustion modes in this research. Under the low stratification condition with $0.2 < \phi < 0.5$, the RANS-WSR method provides a decent prediction. The PaSR approach, which is established from accumulated knowledge, must calibrate an operating model constant for a limited range of conditions; it is a heuristic method. Across all SOIs, this technique does not give superior predictability. In the PPC engine's real performance, depending on load and required EGR conditions, we can divide it into two cases: low load cases and higher load cases. Despite being very behind in SOI time, all the lean fuel mixtures can burn to "stratified HCCI" in low-load cases. Locally rich mixes will begin to appear in higher load cases, resulting in a combination of premixed and no premixed. Based on the simulations performed, issues that need to be further considered are as follows:

- More research and testing are required to achieve more efficient and advanced CFD models, for example, based on tabulation.
- Diesel injection research using dual injection strategies should be carried on to study air intake rates and soot oxidation under various circumstances.

References

An Y. et al., 2017, Analysis of transition from HCCI to CI via PPC with low octane gasoline fuels using optical diagnostics and soot particle analysis, SAE Technical Paper.

Beatrice C., Del Giacomo N., and Guido C., 2009, Benefits and drawbacks of compression ratio reduction in PCCI combustion application in an advanced LD diesel engine, SAE Int. J. Engines, vol. 2, no. 1, pp. 1290–1303.

Bhagatwala A., Sankaran R., Kokjohn S., and Chen J. H. , 2015, Numerical investigation of spontaneous flame propagation under RCCI conditions, Combust. Flame, vol. 162, no. 9, pp. 3412–3426.

Bhave N. A., Gupta M. M., and Joshi S. S. , 2020, Effect of Brown's gas addition on combustion and emissions of homogeneous charge compression ignition engine, Energy Sources, Part A Recover. Util. Environ. Eff., pp. 1–16.

Bhiogade G. E., Sunheriya N., and Suryawanshi J. G. , 2017, Investigations on Premixed Charge Compression Ignition (PCCI) Engines: A Review, in Fluid Mechanics and Fluid Power–Contemporary Research, Springer, pp. 1455–1463.

Bhurat S., Pandey S., Chintala V., Jaiswal M., and Kumar A. , 2021, Investigation of partially pre-mixed charge compression ignition engine characteristics implemented with toroidal combustion chamber and exhaust gas recirculation, Energy Sources, Part A Recover. Util. Environ. Eff., pp. 1–19.

Bilger R. W., Pope S. B., Bray K. N. C., and Driscoll J. F. , 2005, Paradigms in turbulent combustion research, Proc. Combust. Inst., vol. 30, no. 1, pp. 21–42.

Chomiak J. and Karlsson A. , 1996, Flame liftoff in diesel sprays, in Symposium (International) on Combustion, vol. 26, no. 2, pp. 2557–2564.

D'ambrosio S. and Ferrari A. , 2015, Effects of exhaust gas recirculation in diesel engines featuring late PCCI type combustion strategies, Energy Convers. Manag., vol. 105, pp. 1269–1280.

D'Ambrosio S., Iemmolo D., Mancarella A., and Vitolo R. , 2016, Preliminary optimization of the PCCI combustion mode in a diesel engine through a design of experiments, Energy Procedia, vol. 101, pp. 909–916.

Dumitrescu C. E., Stuart Neill W., Guo H., Hosseini V., and Chippior W. L. , 2012, Fuel property effects on PCCI combustion in a heavy-duty diesel engine, J. Eng. gas turbines power, vol. 134, no. 5.

Egüz U., Leermakers N., Somers B., and Goey P. de, 2014, Modeling of PCCI combustion with FGM tabulated chemistry, Fuel, vol. 118, pp. 91–99.

Elkelawy M. et al. , 2021, Influence of lean premixed ratio of PCCI-DI engine fueled by diesel/biodiesel blends on combustion, performance, and emission attributes; a comparison study, Energy Convers. Manag. X, vol. 10, p. 100066.

Elzahaby A. M., Elkelawy M., Bastawissi H. A.-E., El_Malla S. M., and Naceb A. M. M. , 2018, Kinetic modeling and experimental study on the combustion, performance and emission characteristics of a PCCI engine fueled with ethanol-diesel blends, Egypt. J. Pet., vol. 27, no. 4, pp. 927–937.

Ewphun P.-P., Otake M., Nagasawa T., Kosaka H., and Sato S. , 2020, Combustion Characteristic of Offset Orifice Nozzle Under Multi Pulse Ultrahigh Pressure Injection and PCCI Combustion Conditions, SAE Int. J. Adv. Curr. Pract. Mobil., vol. 2, no. 2019-32–0522, pp. 1002–1012.

Fukushima N. et al. , 2015, Combustion regime classification of HCCI/PCCI combustion using Lagrangian fluid particle tracking, Proc. Combust. Inst., vol. 35, no. 3, pp. 3009–3017.

Fuyuto T., Taki M., Ueda R., Hattori Y., Kuzuyama H., and Umehara T. , 2014, Noise and emissions reduction by second injection in diesel PCCI combustion with split injection, SAE Int. J. Engines, vol. 7, no. 4, pp. 1900–1910.

Hanson R. M., Kokjohn S. L., Splitter D. A., and Reitz R. D. , 2010, An experimental investigation of fuel reactivity controlled PCCI combustion in a heavy-duty engine, SAE Int. J. engines, vol. 3, no. 1, pp. 700–716.

Hoang L. V., Nguyen D. C., Truong T. H., Le H. C., and Nguyen M. N. , 2022, Laminar Flame Characteristics of 2,5-Dimethylfuran (DMF) Biofuel: A Comparative Review with Ethanol and Gasoline, Int. J. Renew. Energy Dev., vol. 11, no. 1, pp. 237–254, doi: 10.14710/ijred.2022.42611.

Ibron C., Jangi M., and Bai X. S. , 2019, Effects of in-cylinder flow simplifications on turbulent mixing at varying injection timings in a piston bowl ppc engine, SAE Tech. Pap., vol. 2019, p. 220.

Jain A., Singh A. P., and Agarwal A. K. , 2017, Effect of fuel injection parameters on combustion stability and emissions of a mineral diesel fueled partially premixed charge compression ignition (PCCI) engine, Appl. Energy, vol. 190, pp. 658–669.

Jia M., Li Y., Xie M., and Wang T. , 2013, Numerical evaluation of the potential of late intake valve closing strategy for diesel PCCI (premixed charge compression ignition) engine in a wide speed and load range, Energy, vol. 51, pp. 203–215.

Jia M., Xie M., Wang T., and Peng Z. , 2011, The effect of injection timing and intake valve close timing on performance and emissions of diesel PCCI engine with a full engine cycle CFD simulation, Appl. Energy, vol. 88, no. 9, pp. 2967–2975.

Kanda T., Hakozaki T., Uchimoto T., Hatano J., Kitayama N., and Sono H. , 2005, PCCI operation with early injection of conventional diesel fuel, SAE Trans., pp. 584–593.

Karthickeyan V., Thiyagarajan S., and Ashok B. , 2020, Investigation of alternative fuels as low reactivity fuel in port-charged compression ignition (PCCI) engine, in Recent Technologies for Enhancing Performance and Reducing Emissions in Diesel Engines, IGI Global, pp. 211–233.

Kiplimo R., Tomita E., Kawahara N., and Yokobe S. , 2012, Effects of spray impingement, injection parameters, and EGR on the combustion and emission characteristics of a PCCI diesel engine, Appl. Therm. Eng., vol. 37, pp. 165–175.

Kokjohn S. L., Hanson R. M., Splitter D. A., and Reitz R. D. , 2010, Experiments and modeling of dual-fuel HCCI and PCCI combustion using in-cylinder fuel blending, SAE Int. J. Engines, vol. 2, no. 2, pp. 24–39.

Liang Q., Han D., Cao Z., and Du J. , 2021, Studies on kinetic and reaction mechanism of oil rolling sludge under a wide temperature range, Energy Sources, Part A Recover. Util. Environ. Eff., pp. 1–13.

Lo¨ rstad D. et al. , 2010, Experimental and LES investigation of a SGT-800 burner in a combustion rig, in Turbo Expo: Power for Land, Sea, and Air, vol. 43970, pp. 549–561.

Lundgren M. , 2017, Optical Diagnostics of Gasoline Compression Ignition: HCCI-PPC-Diffusion Combustion. Lund University.

Maghbouli A., Lucchini T., D'Errico G., and Onorati A. , 2015, Effects of grid alignment on modeling the spray and mixing process in direct injection diesel engines under non-reacting operating conditions, Appl. Therm. Eng., vol. 91, pp. 901–912.

Mao G., Zhang C., Shi K., and Wang P. , 2019, Prediction of the performance and exhaust emissions of ethanol-diesel engine using different neural network, Energy Sources, Part A Recover. Util. Environ. Eff., pp. 1–15.

Mei D., Yue S., Zhao X., Hielscher K., and Baar R. , 2017, Effects of center of heat release on combustion and emissions in a PCCI diesel engine fuelled by DMC-diesel blend, Appl. Therm. Eng., vol. 114, pp. 969–976.

Murata Y. et al. , 2009, Miller-PCCI combustion in an HSDI diesel engine with VVT, SAE Int. J. Engines, vol. 1, no. 1, pp. 444–456.

Musculus M. P. B., Miles P. C., and Pickett L. M. , 2013, Conceptual models for partially premixed low-temperature diesel combustion, Prog. energy Combust. Sci., vol. 39, no. 2–3, pp. 246–283.

Natarajan S., Shankar S. A., and Sundareswaran A. U. M. , 2017, Early injected PCCI engine fuelled with bio ethanol and diesel blends–an experimental investigation, Energy Procedia, vol. 105, pp. 358–366.

Nibin M., Raj J. B., and Geo V. E. , 2021, Experimental studies to improve the performance, emission, and combustion characteristics of wheat germ oil fuelled CI engine using bioethanol injection in PCCI mode, Fuel, vol. 285, p. 119196.

Norhafana M. et al. , 2018, A review of the performance and emissions of nano additives in diesel fuelled compression ignition-engines, in IOP Conference Series: Materials Science and Engineering, vol. 469, no. 1, p. 12035.

Pandey S. K., Akella S. R. S., and Ravikrishna R. V, 2018, Novel fuel injection strategies for PCCI operation of a heavy-duty turbocharged diesel engine, Appl. Therm. Eng., vol. 143, pp. 883–898.

Pandey S., Bhurat S. S., and Kunwer R. , 2021, Investigation of fumigation of ethanol and exhaust gas recirculation on combustion and emission characteristics of partially premixed charge compression-ignition engine, Energy Sources, Part A Recover. Util. Environ. Eff., pp. 1–15.

Park H., Kim J., and Bae C. , 2015, Effects of hydrogen ratio and EGR on combustion and emissions in a hydrogen/diesel dual-fuel PCCI engine, SAE Technical Paper.

Parks J. E. II et al., Emissions from premixed charge compression ignition (PCCI) combustion and affect on emission control devices, Catal. Today, vol. 151, no. 3–4, pp. 278–284, 2010.

Parthasarathy M., Ramkumar S., Elumalai P. V, Nachippan M. N., and Dhinesh B. , 2020, Control strategies on HCCI engine performance and emission characteristics by combined effect of exhaust gas recirculation with blend of biodiesel and N-Heptane, ENERGY SOURCES PART A-RECOVERY Util. Environ. Eff..

Pei Y. et al. , 2015, Large eddy simulation of a reacting spray flame with multiple realizations under compression ignition engine conditions, Combust. Flame, vol. 162, no. 12, pp. 4442–4455.

Prikhodko V. Y., Pihl J. A., Lewis S. A., and Parks J. E. , 2012, Hydrocarbon fouling of SCR during PCCI combustion, SAE Int. J. Engines, vol. 5, no. 3, pp. 947–957.

Rohani B., Park S. S., and Bae C. , 2016, Effect of injection strategy on smoothness, emissions and soot characteristics of PCCI-conventional diesel mode transition, Appl. Therm. Eng., vol. 93, pp. 1033–1042.

Sabelnikov V. and Fureby C. , 2013, LES combustion modeling for high Re flames using a multi-phase analogy, Combust. Flame, vol. 160, no. 1, pp. 83–96.

Salahi M. M. and Gharehghani A. , 2019, Control of combustion phasing and operating range extension of natural gas PCCI engines using ozone species, Energy Convers. Manag., vol. 199, p. 112000.

Sankaralingam R. K., Ferroskhan S. I., and Venugopal T. , 2018, Experimental studies on premixed charge compression ignition (PCCI) engine using port injection of heated diesel, J Eng Sci Technol, vol. 13, no. 11, pp. 3457–3472.

Sathishkumar S. and Mohamed Ibrahim M. , 2021, An experimental study on the effect of injection pressure on diesel PCCI engine, Int. J. Ambient Energy, no. just-accepted, pp. 1–31.

Schmitt F. G. , 2007, About Boussinesq's turbulent viscosity hypothesis: historical remarks and a direct evaluation of its validity, Comptes Rendus Mécanique, vol. 335, no. 9–10, pp. 617–627.

Shim E., Park H., and Bae C. , 2020, Comparisons of advanced combustion technologies (HCCI, PCCI, and dual-fuel PCCI) on engine performance and emission characteristics in a heavy-duty diesel engine, Fuel, vol. 262, no. July 2019, p. 116436, doi: 10.1016/j.fuel.2019.116436.

Singh A. P. and Agarwal A. K. , 2017, CI/PCCI Combustion Mode Switching of Diesohol Fuelled Production Engine, SAE Technical Paper.

Singh A. P., Bajpai N., and Agarwal A. K. , 2018, Combustion mode switching characteristics of a medium-duty engine operated in compression ignition/PCCI combustion modes, J. Energy Resour. Technol., vol. 140, no. 9.

Singh A. P., Jain A., and Agarwal A. K. , 2017, Fuel-Injection Strategy for PCCI Engine Fueled by Mineral Diesel and Biodiesel Blends, Energy & Fuels, vol. 31, no. 8, pp. 8594–8607.

Singh A. P., Kumar V., and Agarwal A. K. , 2020, Evaluation of comparative engine combustion, performance and emission characteristics of low temperature combustion (PCCI and RCCI) modes, Appl. Energy, vol. 278, p. 115644.

Soloiu V. et al. , 2018, LTC (low-temperature combustion) analysis of PCCI (premixed charge compression ignition) with n-butanol and cotton seed biodiesel versus combustion and emissions characteristics of their binary mixtures, Renew. energy, vol. 123, pp. 323–333.

Soloiu V., Muinos M., and Harp S. , 2015, Investigation of Dual Fuel PCCI (PFI of n-Butanol and DI-ULSD) Compared with DI of Binary Mixtures of the Same Fuels in an Omnivorous Diesel Engine, SAE Technical Paper.

Sone K. and Menon S. , 2003, Effect of subgrid modeling on the in-cylinder unsteady mixing process in a direct injection engine, J. Eng. Gas Turbines Power, vol. 125, no. 2, pp. 435–443.

Splitter D., Kokjohn S., Rein K., Hanson R., Sanders S., and Reitz R. , 2010, An optical investigation of ignition processes in fuel reactivity controlled PCCI combustion, SAE Int. J. Engines, vol. 3, no. 1, pp. 142–162.

Srihari S., Thirumalini S., and Prashanth K. , 2017, An experimental study on the performance and emission characteristics of PCCI-DI engine fuelled with diethyl ether-biodiesel-diesel blends, Renew. Energy, vol. 107, pp. 440–447.

Torregrosa A. J., Broatch A., García A., and Mónico L. F. , 2013, Sensitivity of combustion noise and NOx and soot emissions to pilot injection in PCCI Diesel engines, Appl. Energy, vol. 104, pp. 149–157.

Van Alstine D. G., Kocher L. E., Koeberlein E., Stricker K., and Shaver G. M. , 2012, Control-oriented PCCI combustion timing model for a diesel engine utilizing flexible intake valve modulation and high EGR levels, in 2012 American Control Conference (ACC), pp. 2060–2065.

Wang Z. et al. , 2019, Simultaneous 36 kHz PLIF/chemiluminescence imaging of fuel, CH2O and combustion in a PPC engine, Proc. Combust. Inst., vol. 37, no. 4, pp. 4751–4758.

Yoon S. H., Kim H. J., and Park S. , 2018, Study on optimal combustion strategy to improve combustion performance in a single-cylinder PCCI diesel engine with different combustion chamber geometry, Appl. Therm. Eng., vol. 144, pp. 1081–1090.

Zehni A., Balazadeh N., Hajibabaei M., and Poorghasemi K. , 2020, Numerical study of the effects of split injection strategy and swirl ratio for biodiesel PCCI combustion and emissions, Propuls. Power Res., vol. 9, no. 4, pp. 355–371.

Zehni A., Saray R. K., and Poorghasemi K. , 2017, Numerical comparison of PCCI combustion and emission of diesel and biodiesel fuels at low load conditions using 3D-CFD models coupled with chemical kinetics, Appl. Therm. Eng., vol. 110, pp. 1483–1499.

Zhang F., Yu R., and Bai X.-S. , 2015, Direct numerical simulation of PRF70/air partially premixed combustion under IC engine conditions, Proc. Combust. Inst., vol. 35, no. 3, pp. 2975–2982.

Zhang F., Yu R., Bai X. S., Yao M., and Peng Z. , 2017, Direct numerical simulation of flame/spontaneous ignition interaction fueled with hydrogen under SACI engine conditions, Int. J. Hydrogen Energy, vol. 42, no. 6, pp. 3842–3852.

Zhang Y., Jia M., Liu H., Xie M., and Wang T. , 2015, Investigation of the characteristics of fuel adhesion formed by spray/wall interaction under diesel premixed charge compression ignition (PCCI) relevant conditions, At. Sprays, vol. 25, no. 11.

Zhang Y., Jia M., Liu H., Xie M., Wang T., and Zhou L. , 2014, Development of a new spray/wall interaction model for diesel spray under PCCI-engine relevant conditions, At. Sprays, vol. 24, no. 1.

Zheng Z. et al. , 2019, Study on the flame development patterns and flame speeds from homogeneous charge to stratified charge by fueling n-heptane in an optical engine, Combust. Flame, vol. 199, pp. 213–229.